Monte-Carlo simulation of anisotropic diffusion measured by elliptical photobleaching in three dimensions

We simulate fluorescence recovery curves by full 3-d analysis of anisotropic diffusion using a Monte-Carlo approach. Initial particle positions were generated randomly in which each particle can move to one of the 8 adjacent lattice points during a time step, with imposed periodic boundary conditions and reflective boundary condition at the tissue surface. Distances between the lattice points in the x, y and z directions are $\Delta x = \sqrt{2D_x \Delta t}$, $\Delta y = \sqrt{2D_y \Delta t}$, and $\Delta z = \sqrt{2D_z \Delta t}$, respectively. Random numbers were generated using L'Ecuyer with Bays-Durham shuffle and added safeguards, which has a period $>2^{18}$.

After simulating the Brownian motions of all particles, the fluorescence recovery curve was computed by bleaching a subset of particles at their initial positions, and calculating the fluorescence emitted from unbleached particles diffusing into the illumination volume.

Particles are bleached according to the probability of photobleaching given by,

$$P_{pb}(x, y, z) = 1 - \exp\left[-KI(x, y, z)\right] \qquad \text{(S1)}$$

where K is a bleaching factor and $I(x, y, z)$ is the three-dimensional profile of the illumination intensity. $P_{pb}(x_i, y_i, z_i)$ for each particle i is compared with a random number distributed uniformly between 0 and 1 to determine whether particle i is photobleached. If $P_{pb}(x_i, y_i, z_i)$ is greater than the random number, bleaching occurs and the excited particle becomes permanently unexcitable. K was chosen to produce an ~50% reduction in fluorescence immediately following bleaching.

Computations were done using three different illumination profiles $I(x, y, z)$: an exact form of the diffraction-limited intensity distribution ('true illumination profile'), a

3-d Gaussian distribution ('3-d Gaussian profile') that approximates the true illumination profile, and an 'experimentally-measured' profile.

True illumination profile:

$$I(x,y,z) = I_0 \frac{w_{x0}w_{y0}}{w_x(z)w_y(z)} \exp\left(-2\left(\frac{x^2}{w_x^2(z)} + \frac{x^2}{w_y^2(z)}\right)\right) \quad \text{(S2)}$$

$$w_x(z) = w_{x0}\sqrt{1+\left(\lambda z/\pi w_{x0}^2\right)^2}, \quad w_y(z) = w_{y0}\sqrt{1+\left(\lambda z/\pi w_{y0}^2\right)^2}$$

where I_0 is the maximum illumination intensity, w_{x0} and w_{y0} are the beam waists in the x and y dimensions, respectively, at which the detected fluorescence has $1/e^2$ of its peak intensity, and λ is illumination wavelength.

3-d Gaussian profile:

$$I(x,y,z) = I_0 \exp\left(-2\left(\frac{x^2}{w_{x0}^2} + \frac{y^2}{w_{y0}^2}\right) - \frac{2z^2}{w_{z0}^2}\right) \quad \text{(S3)}$$

Emitted fluorescence from an excited particle *i* was assumed to be proportional to $I(x_i, y_i, z_i)$. A laser intensity profile for detection, *D(x, y, z)*, is defined by the product of the illumination profile and the collection efficiency function, *CEF(x, y, z)*, which depends on pinhole size and numerical aperture of the objective.

$$D(x,y,z) = I(x,y,z)CEF(x,y,z) \quad \text{(S4)}$$

The detection profile can be approximated as the 3-d Gaussian profile used for bleaching (Blonk et al., 1993).

Experimentally-measured profile: The experimentally-measured illumination profile $I(x_i, y_i, z_i)$ of the 3:1 ellipse was obtained as depicted in Figure S1 left. A turbid non-fluorescent solution (5% non-fat milk powder in water) was used to approximately match

the turbidity of spinal cord at excitation/emission wavelengths. To simulate the experimental situation for each solution depth (z) the elliptical spot (produced by the same cylindrical optics used in the study) was focused on the top surface of the milk layer and the light emerging at different points (x,y) from the bottom surface of the milk layer was detected from below by scanning a fiberoptic with 1-2 μm tip diameter using a 2-d micropositioner. The measured values were then used in an interpolated look-up table in the computation.

The experimentally measured detection efficiency, *CEF(x, y, z)*, was obtained as shown in Figure S1 right. A 100x oil immersion objective lens was used to focus green light at the bottom surface of a non-fluorescent turbid solution (turbidity matched to spinal cord) sandwiched between coverslips. The lens was mounted on a 2-d micropositioner to permit x-y scanning. Light emerging at the top surface of the milk fluid layer was detected by the pinhole / photomultiplier detection system used for the elliptical photobleaching studies. Measurements were taken at different solution depths (z).

The time course of fluorescence recovery after photobleaching, $F(t)$, was calculated by summing fluorescence signals from all unbleached particles at each time step.

$$F(t)/F(\ \ ) = \prod_{i=1}^{N} P(i)D(x_i, y_i, z_i) \qquad \text{(S5)}$$

where $F(\ \ )$ is fluorescence at full recovery, N is the total number of particles, and $P(i)$ (0 or 1) is determined from the comparison of $P_{pb}(x_i, y_i, z_i)$ with a random number selected between 0 and 1.

To display fluorescence recovery curves, we use the fractional form $f(t)$, defined as,

$$f(t) = \frac{F(t) - F(0)}{F(\infty) - F(0)} \tag{S6}$$

where $F(0)$ is initial fluorescence after photobleaching.

The noise in simulated recovery curves and the total number of particles used for the simulation was greatly reduced by following the bleached particles moving out of the illumination volume (rather than the many more unbleached particles). Since the sum of the concentrations of the bleached and unbleached particles is constant, we can trace the bleached particles instead of unbleached particles (Saxton, 2001). Using this approach, periodic boundary conditions are not required for the simulation. Initially, particles are distributed randomly inside the bleaching volume defined as

$$x^2/(2w_{x0})^2 + y^2/(2w_{y0})^2 + z^2/(2w_{z0})^2 < 1. \tag{S7}$$

To validate the computational accuracy, we compared the simulated recovery curve with the analytical solution given for the three-dimensional photobleaching measurement of isotropic diffusion with same illumination and detection profiles (Blonk et al., 1993; Brown et al., 1999): $I(x,y,z) = I_0 \exp[-(x^2 + y^2)/w_0^2 - z^2/w_{z0}^2]$. The fluorescence recovery is given by,

$$F(t)/F(\infty) = \sum_{n=0} \frac{(-K)^n}{n!} \frac{1}{(1 + n + 8nDt/w_0^2)} \frac{1}{\sqrt{(1 + n + 8nDt/w_{z0}^2)}}. \tag{S8}$$

Figure S2 shows that computed $f(t)$ (solid lines) is in close agreement with the analytical solution (open dots with black line). As predicted from the statistical theory, deviations from the analytical solution were reduced with increasing particle number (Figure S2 A). Averaging several simulated recovery curves further reduced the deviation (Figure S2 B).

For the simulation of elliptical photobleaching experiments in anisotropic media, the distance between neighboring lattices points in each direction was varied from 0.14 to 0.45 μm and the time step was 1 ms. The bleaching factor K was chosen to produce a reduction of ~50% in fluorescence immediately following bleaching. To obtain good statistical convergence, 10^4 particles were used to generate each simulated recovery curve. Ratios of fluorescence recovery half-times were computed with the ellipse in orientation b (long axis in y direction) *vs.* orientation a (long axis in x direction), $t_{1/2}^{(b)}/ t_{1/2}^{(a)}$, as a function of D_y/D_x ($D_z = D_x$) for the 30 × 10 μm^2 ellipse. The fluorescence recovery half-time for each case was obtained from 10 recovery curves.

Figure S3 A shows the simulated fluorescence recovery curves for the case of three-dimensional elliptical photobleaching with the ellipse in orientation b *vs.* orientation a, and for different D_y/D_x. Figure S3 B shows the ratio of recovery half-times ($t_{1/2}^{(b)}/ t_{1/2}^{(a)}$) computed as a function of D_y/D_x for 3:1 ratio of elliptical beam waists in the x and y dimensions. Computed $t^{(b)}_{1/2}/ t^{(a)}_{1/2}$ vs. (D_y/D_x) for the 3-d and 2-d computations were very similar, validating the 2-d numerical solution for the system used here. The 2-d is a good approximation here because fluorophore diffusion from below is minimal in spinal white matter where D_z is small (~D_x). In addition, the confocal optics minimized the z-detection depth, and the objective and cylindrical lenses were chosen to achieve a near-constant cylindrical beam profile for many microns in the z-direction as shown in Figure S3.

References

Blonk JCG, Don A, van Aalst H, Birmingham JJ (1993) Fluorescence photobleaching recovery in the confocal scanning light microscope. *J Microscopy* 169:363-374.

Brown EB, Wu ES, Zipfel W, Webb WW (1999) Measurement of molecular diffusion in solution by multiphoton fluorescence photobleaching recovery. *Biophys J* 77:2837-2849.

Saxton MJ (2001) Anomalous subdiffusion in fluorescence photobleaching recovery; a Monte Carlo study. *Biophys J* 81:2226-2240.

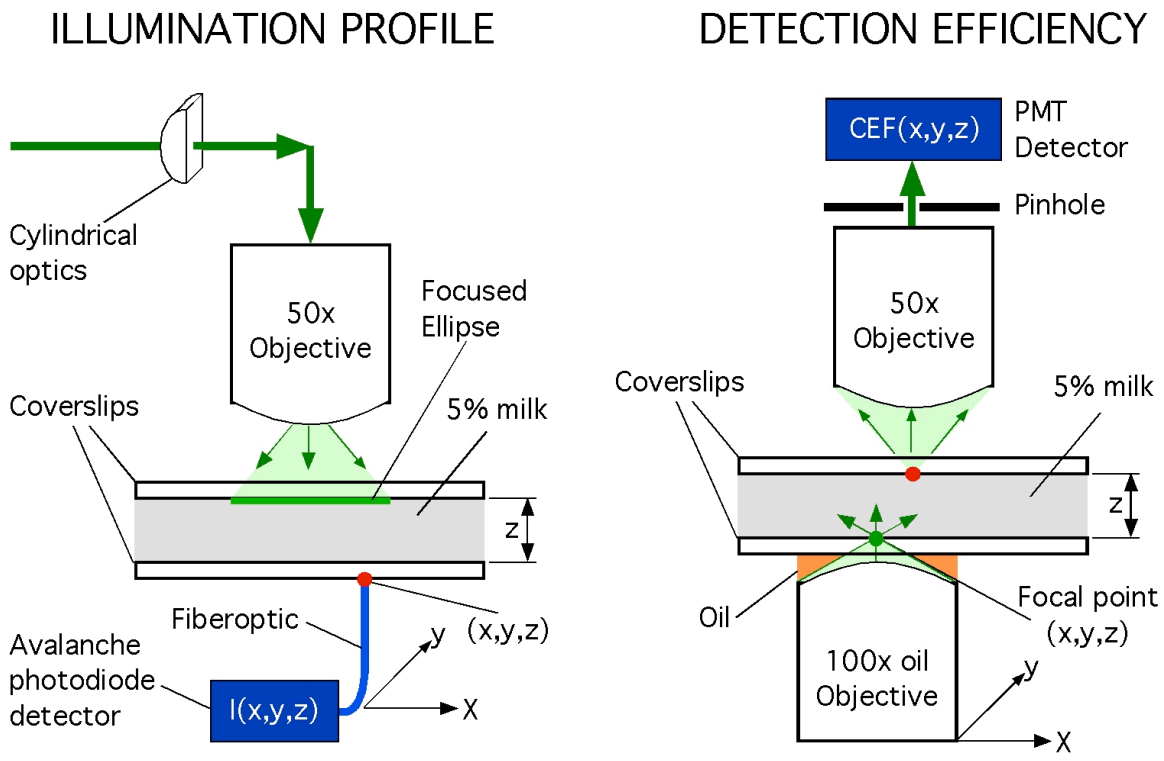

Figure S1. Experimental setup for determining *(left)* the illumination profile I(x,y,z), and *(right)* the detection efficiency CEF(x,y,z). 5% milk was sandwiched between two coverslips to simulate the scattering properties of brain. The thickness of the milk layer (z) was varied by moving the lower (for illumination profile) or upper (for detection efficiency) coverslips using a micromanipulator. *(Left)* The 3:1 ellipse was focused on the undersurface of the top coverslip using the elliptical optics illumination system. The illumination at different (x,y,z) coordinates was determined by using a micro-fiberoptic and an avalanche photodiode detector. *(Right)* A 100□ oil objective was used to focus light onto the top surface of the bottom coverslip. For different (x,y,z), light collected by the 50x objective and detected by a photomultiplier tube (PMT) after passing through the pinhole used to obtain partial confocal optics.

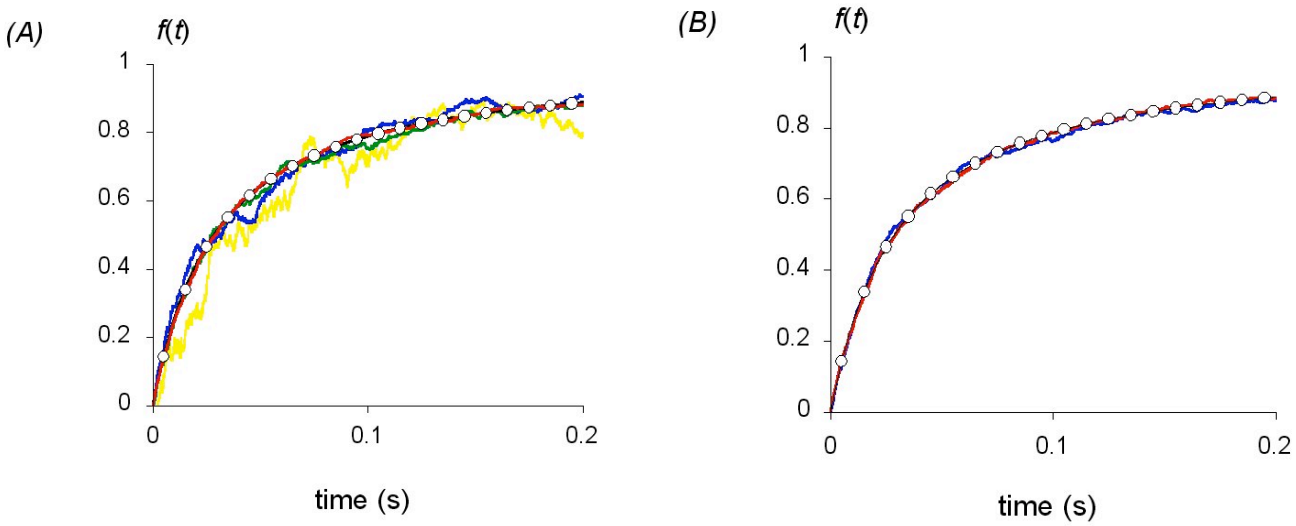

Figure S2. Comparison of simulated recovery curves (*solid lines*) with analytical solution (*open dots with black line*) for the case of three-dimensional photobleaching in isotropic media. Computations done with the same 3-d Gaussian profile for illumination and detection; $D = 10^{-7}$ cm^2/s, $w_0 = 1$ μm, $w_{z0} = 5$ μm, $K = 2.5$ (50% bleaching). (A) Effect of particle numbers (*yellow*: 10^3, *blue*: 5×10^3, *green*: 10^4 and *red*: 5×10^4 particles). (B) Effect of averaging (*blue* and *red* for mean recovery curves from 5 and 10 recovery curves simulated using 10^4 particles, respectively).

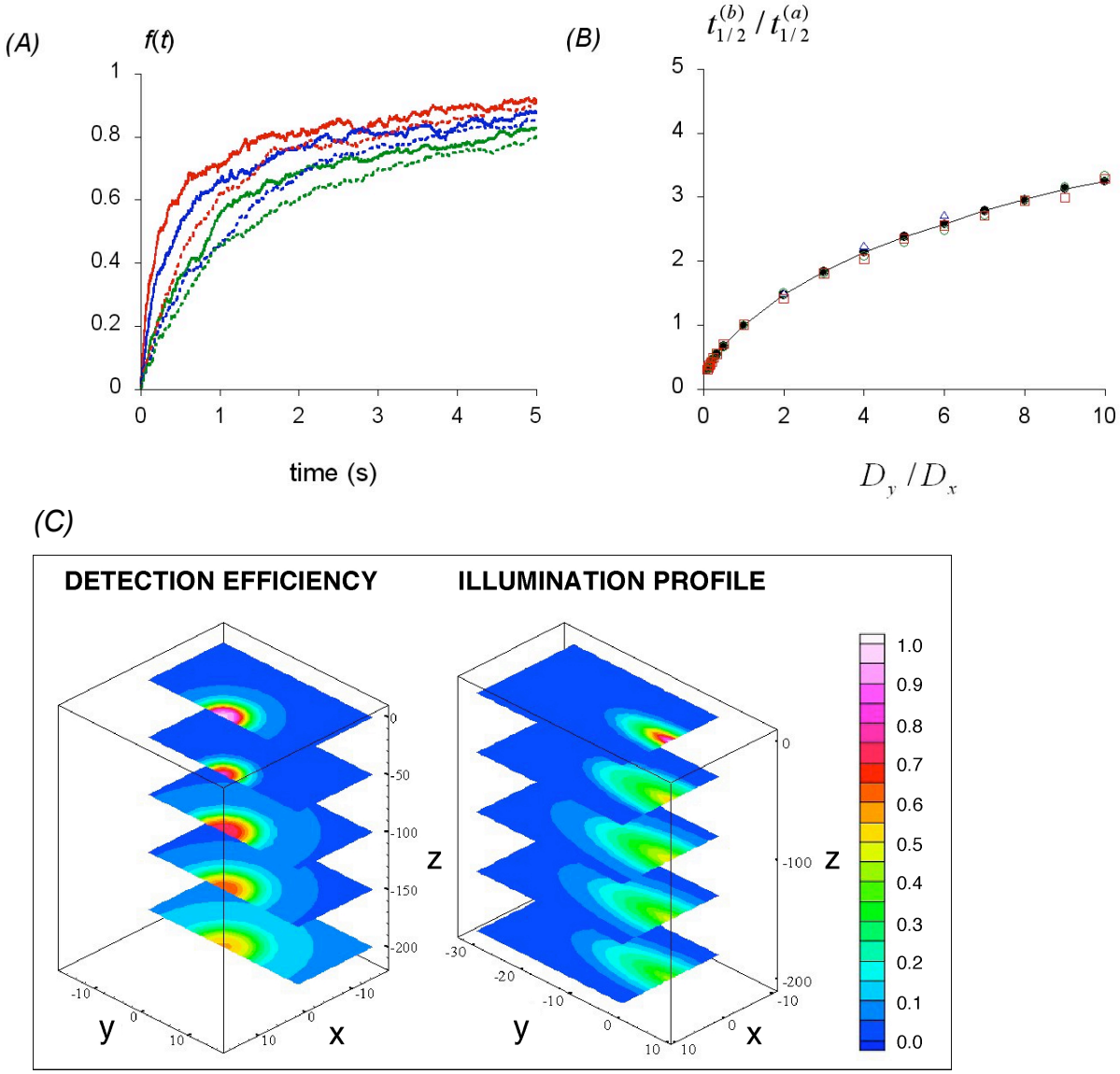

Figure S3. (A) Simulated fluorescence recovery curves for three-dimensional elliptical photobleaching in anisotropic media with ellipse in orientation b (long axis in *y* direction; *dotted lines*) *vs.* orientation a (long axis in *x* direction; *solid lines*). Monte Carlo simulations done with the same 3-d Gaussian profile for illumination and detection; $D_y/D_x = 2$ (*green*), 4 (*blue*) and 8 (*red*), $D_z = D_x = 10^{-7}$ cm^2/s; $w_{x0} = 15$ μm, $w_{y0} = w_{z0} = 5$ μm, $K = 2.5$ (50% bleaching). (B) Ratio of fluorescence recovery half-times with ellipse in orientation b *vs.* orientation a, $t_{1/2}^{(b)}/ t_{1/2}^{(a)}$, as a function of D_y/D_x. $D_z = D_x = 10^{-7}$ cm^2/s for $D_y \geq D_x$, $D_z = D_y = 10^{-7}$ cm^2/s for $D_y < D_x$; $w_{x0} = 15$ μm, $w_{y0} = w_{z0} = 5$ μm. Computations done for true illumination profile (*square*; $K = 1.6$), 3-d Gaussian profile (*circle*; $K = 2.5$), and experimentally-measured illumination profile; filled circles and triangles show computed D_y/D_x for a flat elliptical illumination profile and a 2-d Gaussian beam profile for the 3:1 ellipse, respectively. (C) 3-d contour plots of experimentally-measured, normalized detection efficiency and illumination profiles.